King Saud University

Arabian Journal of Chemistry

www.ksu.edu.sa
www.sciencedirect.com

ORIGINAL ARTICLE

Bio-supported of Cu nanoparticles on the surface of Fe$_3$O$_4$ magnetic nanoparticles mediated by *Hibiscus sabdariffa* extract: Evaluation of its catalytic activity for synthesis of pyrano[3,2-c]chromenes and study of its anti-colon cancer properties

Chengzheng Wang [a], Bikash Karmakar [b,*], Nasser S. Awwad [c], Hala A. Ibrahium [d,e], Attalla F. El-kott [d,f], Mohamed M. Abdel-Daim [g,h], Atif Abdulwahab A. Oyouni [i,j], Osama Al-Amer [j,k], Gaber El-Saber Batiha [l]

[a] *Department of General Surgery, The People's Hospital of Jianhu, Yancheng 224700, China*
[b] *Department of Chemistry, Gobardanga Hindu College, 24 Parganas (North), India*
[c] *Department of Chemistry, Faculty of Science, King Khalid University, P.O. Box 9004, Abha 61413, Saudi Arabia*
[d] *Biology Department, College of Science, King Khalid University, Abha 61421, Saudi Arabia*
[e] *Department of Semi Pilot Plant, Nuclear Materials Authority, P.O. Box 530, El Maadi, Egypt*
[f] *Department of Zoology , College of Science, Damanhour University, Damanhour 22511, Egypt*
[g] *Pharmaceutical Sciences Department, Pharmacy Program, Batterjee Medical College, P.O. Box 6231, Jeddah 21442, Saudi Arabia*
[h] *Pharmacology Department, Faculty of Veterinary Medicine, Suez Canal University, Ismailia 41522, Egypt*
[i] *Department of Biology, Faculty of Sciences, University of Tabuk, Tabuk, Saudi Arabia*
[j] *Genome and Biotechnology Unit, Faculty of Sciences, University of Tabuk, Tabuk, Saudi Arabia*
[k] *Department of Medical Laboratory Technology, Faculty of Applied Medical Sciences, University of Tabuk, Tabuk, Saudi Arabia*
[l] *Department of Pharmacology and Therapeutics, Faculty of Veterinary Medicine, Damanhour University, Damanhour 22511, AlBeheira, Egypt*

Abstract In this work, we have described the biogenic synthesized copper nanoparticles being supported over plant phytochemicals modified magnetic Fe$_3$O$_4$ nanoparticles. *Hibiscus sabdariffa* extract was used as a green reducing agent and an excellent stabilizer of the synthesized NPs.

* Corresponding author.
 E-mail address: bkarmakar@ghcollege.ac.in (B. Karmakar).
Peer review under responsibility of King Saud University.

ELSEVIER **Production and hosting by Elsevier**

The biomolecules are adorned as a protective shell over the core ferrite NPs. Physicochemical characterization of the as-synthesized Cu-*Hibiscus*@Fe$_3$O$_4$ nanocomposite was carried out through Fourier transformed infrared spectroscopy (FT-IR), electron microscopy (SEM and TEM), energy dispersive X-ray spectroscopy (EDX), elemental mapping (WDX), vibrating sample magnetometer (VSM), X-ray diffraction (XRD) and inductively coupled plasma-optical emission spectroscopy (ICP-OES). The as-synthesized bio-nanomaterial was used as an excellent heterogeneous and magnetically retrievable catalyst in the three-component condensation of 4-hydroxycoumarin, malononitrile and various aldehydes in refluxing aqueous media. A broad range of aromatic aldehydes underwent the reaction to produce diverse pyrano[3,2-c]chromene derivatives in very good yields irrespective of the nature of bearing functional groups or their respective geometrical positions. Due to superparamagentic character, the material was easily magnetically decanted out and recycled for 8 successive times with preservation of its catalytic activity. After the chemical applications we also explored the material biologically in the resistance of human colon cancer and thereby studied the cytotoxicity over two standard cell lines, HT-29 and Caco-2. The conventional MTT assay was carried out over them which revealed an increase in % cell viability dose dependantly. In addition, DPPH radical scavenging test was performed for studying anti-oxidant activity, using BHT as the positive control. The IC50 values observed in the two cell lines were 490.12 µg/ml and 412.23 µg/ml respectively. The results validate the administration of Cu-*Hibiscus*@Fe$_3$O$_4$ as a competent colon protective drug in the clinical trial studies over human.

1. Introduction

In recent times, it has been a continuous trend to develop the functionalized nanomaterials in advanced level to improve their physicochemical, catalytic and biological properties. But, the advent of different efficient physical and chemical methods for the preparation of modified nanomaterials has concurrently elevated the concern of sustainability due to harshness of the protocol as well as the development of hazardous by-products. Hence, there is an obvious requirement for green technology in such processes (Gawande et al., 2013; Sadjadi et al., 2020). Consequently, abundant investigations have been being carried out on the bottom-up synthesis of materials involving functional biomolecules, more precisely, the phytochemicals derived from plant kingdom. Biogenic methodology towards nanomaterials bestows several unique features like tailorable size and uniform shape, great dispersion, outstanding thermal and mechanical stability, large surface to volume ratio, high surface lipophilicity and provision to further surface modifications (Tamoradi et al., 2020; Hemmati et al., 2020). The bio-engineered materials find tremendous significance in different environmental issues, medicinal therapeutics, biomedical implications, sensing, and catalysis (Olivera et al., 2016; Awual et al., 2018; Mohammadi et al., 2020; Aguilera et al., 2019; Esmaeilpour et al., 2018; Lotfi and Veisi, 2019; Ding et al., 2015; Colombo et al., 2012; Cao et al., 2017). Among the different categories of modified nanomaterials, the magnetic core-bioshell type hybrid nanoparticles garners significant importance based on their ease and cost-effective synthesis from cheap raw materials, biocompatibility, excellent support for immobilizing active drug or material, high chemical and mechanical stability, strong magnetic permeability, effortless isolation from the applied systems and reusability with almost unaltered activity (Tamoradi et al., 2020; Veisi et al., 2019; Veisi et al., 2020; Veisi et al., 2018; Maleki et al., 2015; Maleki et al., 2016; Maleki et al., 2016; Maleki and Yeganeh, 2017; Maleki et al., 2018; Maleki et al., 2019; Maleki et al., 2020; Maleki et al., 2018; Rostamnia et al., 2018; Doustkhah et al., 2017). Although different protective shells like graphene derivatives, carbonaceous materials, silica, biopolymers, polyhydroxy surfactants and organic ligands have been reported in recent past in successive catalysis and other applications (Tamoradi et al., 2021; Hemmati et al., 2021; Tamoradi et al., 2021; Tamoradi et al., 2021), implement of plant derived phytochemicals over the core MNPs has been the latest development in view of green and sustainable chemistry. The lipophilic and electron rich environment provided by the oxygenated or nitrogeneous organo-functions also facilitate the confinement of incoming metal ions at the surface and subsequently reduces in a green pathway to the corresponding NPs (Tamoradi et al., 2021; Veisi et al., 2021; Veisi et al., 1983; Adyani and Soleimani, 2019; Rocha-Santos, 2014). Such a bimetallic combination of nanoparticles often demonstrates substantial synergetic effects, particularly in catalysis (Khalilzadeh et al., 2020; Heydari et al., 2019; Rahimi et al., 2020).

In this particular study, we report the biogenic synthesis of Cu NPs immobilized on magnetite nanoparticles using *Hibiscus sabdariffa* flower extract as a green reducing and stabilizing agent (Scheme 1). The as-synthesized Cu-*Hibiscus*@Fe$_3$O$_4$ nanocomposite exhibited excellent potential as a recyclable nanocatalyst towards the pyrano[3,2-c]chromenes by one-pot three-component condensation of various aldehydes, 4-hydroxycoumarin and malononitrile in aqueous media (Scheme 1).

Multicomponent reactions (MCRs) have garnered tremendous attention among organic chemists for designing highly functionalized organic scaffolds and biologically important heterocycles in one-pot atom economical pathway. The methodology is also sustainably viable in terms of simplicity, high yielding and feasible in the formation of complex molecules which have been quite irksome otherwise (Rostamnia
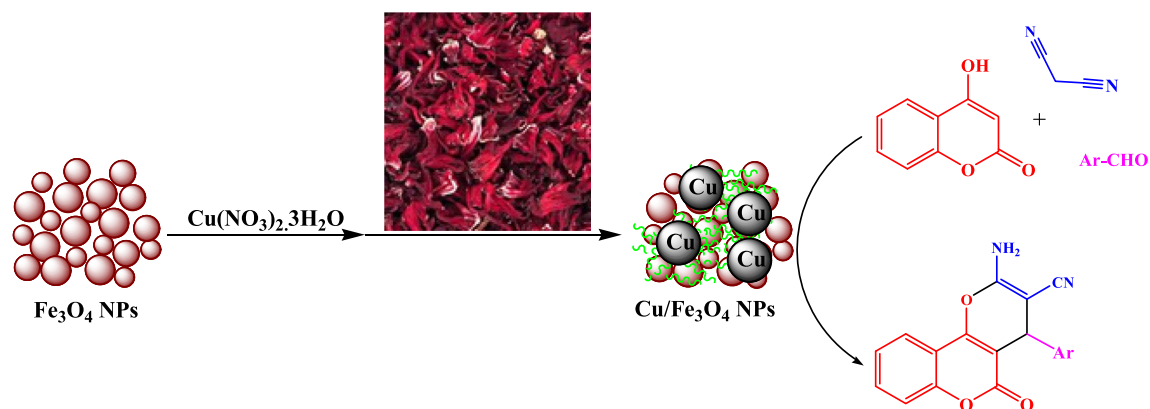
Scheme 1   Schematic green synthesis of magnetic Cu-*Hibiscus*@Fe_3O_4 nanocomposite mediated by *Hibiscus sabdariffa* extract and its applications for synthesis of pyrano[3,2-*c*]chromene derivatives.

et al., 2018; Rostamnia and Xin, 2014; Rostamnia and Doustkhah, 2015).

Chromenes are important classes of biologically relevant oxygenated heterocycle and among them the chemistry of Pyrano[3,2-c]chromene derivatives has received great interest over the last few years. The scaffold constitutes a significant structural component in naturally occurring and synthetically made drug-like molecules displaying broad spectrum of biological activities. They are endowed with wide range of pharmaceutical aspects like antimicrobial, antiviral, antitumor diuretic, analgesic, myorelaxant, anticoagulant, anticancer, antitumor, anti-HIV, anti-infertility, anticancer, antidepressant, antihypertensive, antitubulin and soon. They have potential application in psoriatic and rheumatoid arthritis. Chromenes are known to activate potassium channels and inhibit phosphodiesterase IV and dihydrofolate reductases (Gourdeau et al., 2004; Chetan et al., 2012; Burgard et al., 1999; Evans et al., 1984; Zhang et al., 2016; Mungra et al., 2011; Bonsignore et al., 1993; Saundane et al., 2013; Makawana et al., 2012; Venkatesham et al., 2012; Jagadishbabu and Shivashankar, 2017; Shivashankar et al., 2006; Shivashankar et al., 2007; Maleki et al., 2019; Maleki et al., 2019; Maleki et al., 2017; Maleki et al., 2017). There have been several reports on this synthesis by different research groups following variety of catalysts (Heravi et al., 2008; Khurana et al., 2010; Ghashang et al., 2014; Ghashang et al., 2015; Baziar and Ghashang, 2016; Ghashang, 2016; Ghashang, 2016; Ghashang et al., 2016; Ghashang et al., 2016; Singh et al., 2012; Pradhan et al., 2014; Wang et al., 2010; Vala et al., 2016; Mansoor et al., 2015; Brahmachari and Banerjee, 2014). Nevertheless, despite the significance of the reported procedures for the synthesis of this nucleus, we believe there are ample scopes to develop the protocol, both productively as well as sustainably. The devised methodology involves several benefits like biocompatible green and reusable nanocatalyst, simple chemical procedure, excellent yields in short reaction time, isolation of products by simple filtration without the need of tedious chromatographic methods, isolation of catalyst by magnetic decantation and reusability of catalyst for 8 successive times without considerable leaching of the Cu species.

After the ample chemical appliance of the material, we extended our research towards its biological activities. In recent times, due to high biocompatibility and unique structural features, biogenic modern materials have been extensively used in biomedical arena, particularly in medicinal therapeutics. One of the major applications these materials find in the detection and inhibition of different kind of cancer cells. Colon or colorectal cancer (CRC) is one of the major lethal, invasive and metastatic human gastrointestinal disorders (Dong et al., 2019; Lin et al., 2020). Its morbidity and mortality rate is significantly high, unless being diagnosed in early stage. Nevertheless, clinical surgery, chemotherapy, radio therapy and targeted therapy are the usual treatment protocols against CRC (Han et al., 2019; Valeri, 2019). These procedures are also not hazardless, but involves several drawbacks like swelling of the incision area, nerve damage, hair loss, fatigue, stomach disturbance etc. Accordingly, an alternate formulation method is of great demand having high specificity and efficacy (Abdel-Fattah and Ali, 2018; Patil and Kim, 2017; Bisht and Rayamajhi, 2016; Hassanien et al., 2018). Actually, this has prompted us to use the Cu-*Hibiscus*@Fe_3O_4 nanocomposite as a novel chemotherapeutic material and introduced *in vitro* over two CRC cell lines HT-29 and Caco-2 to study the cytotoxicity and antioxidant potential.

2. Experimental:

2.1. Preparation of *Hibiscus sabdariffa* extract

Hibiscus sabdariffa petals were washed with deionized water and dried at room temperature. 2.0 g of dried flower was added to 50 mL deionized water and heated to 80 °C for 30 min until the solution color changed to light yellow. It was then filtered through Whatman-1 filter paper and maintained at 4 °C for further study.

2.2. Synthesis of the Fe_3O_4 magnetite nanoparticles

Magnetite nanoparticles (Fe_3O_4) were synthesized by co-precipitation of its precursors, namely, $FeSO_4 \cdot 7H_2O$ (4.2 g) and $FeCl_3 \cdot 6H_2O$ (6.1 g) into deionized water (100 mL). Initially, the two salts were dissolved in water and stirred at 90 °C for 30 min which was followed by the dropwise addition of 10 mL anhydrous ammonia. The mixture was stirred at
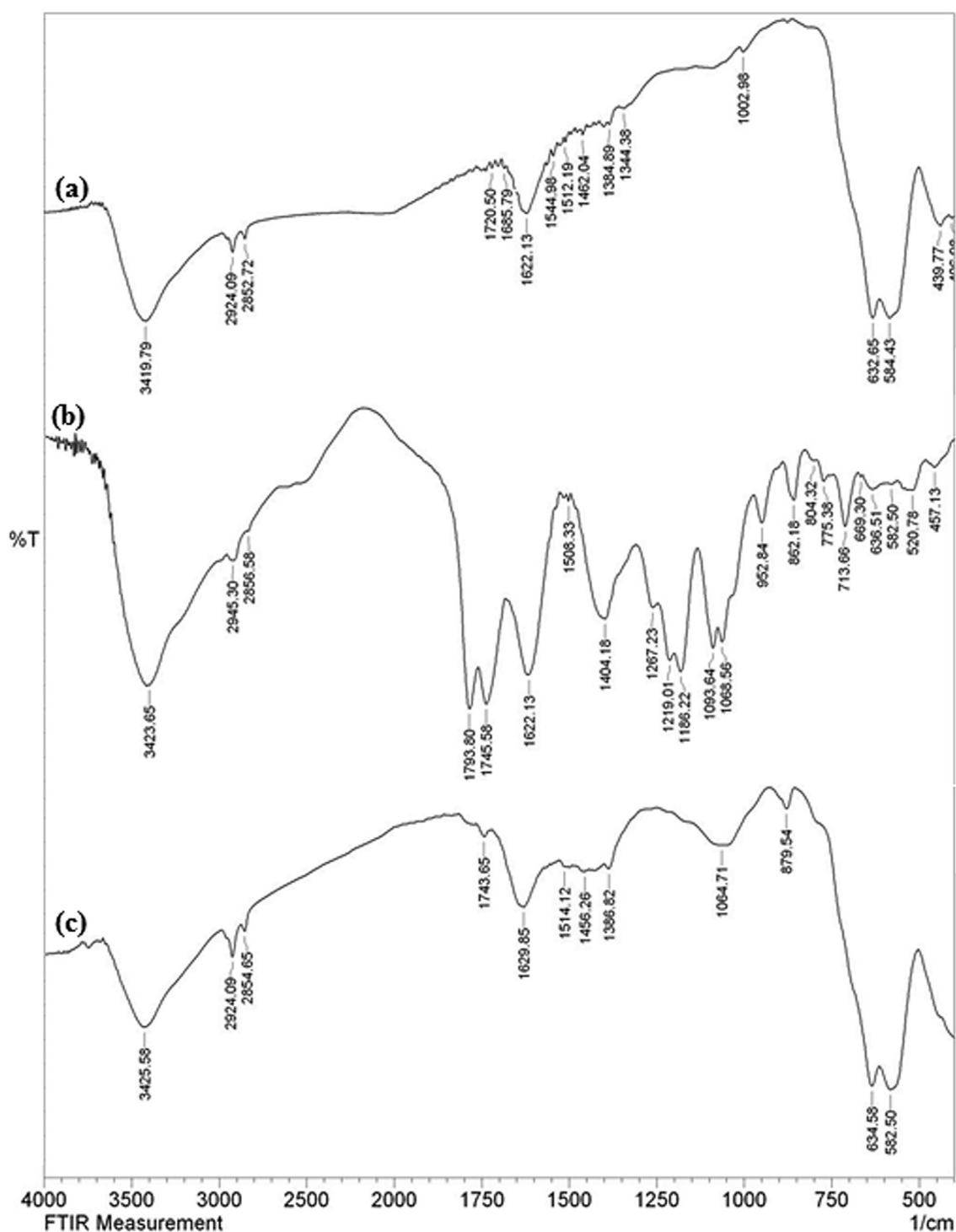
80 °C for 30 min again. The brown colored Fe_3O_4 NPs were retrieved using a strong magnet, washed with deionized water to neutrality and dried at 80 °C.

2.3. Green synthesis of the Cu-*Hibiscus*@/Fe₃O₄ nanoparticles

0.6 g Fe_3O_4 NPs were sonicated in deionized water (100 mL) for 20 min to complete dispersion and then 30 mg $Cu(NO_3)_2$·$3H_2O$ was added to the solution and stirred for 1 h. The prepared flower extract was subsequently added and stirred for 6 h at 100 °C. The Cu-*Hibiscus*@/Fe₃O₄ nanocomposite was

finally separated using magnet, washed by deionized water to neutrality and dried at 60 °C.

2.4. General procedure for synthesis of pyrano[3,2-c]chromene derivatives

A mixture of 4-hydroxycoumarin (1.0 mmol), aromatic aldehyde (1 mmol), and malononitrile (1 mmol) and Cu-*Hibiscus*@/Fe₃O₄ nanocomposite catalyst (20 mg) was refluxed in water (5 mL), for an appropriate time. When the reaction was completed (by TLC), the catalyst was isolated with an
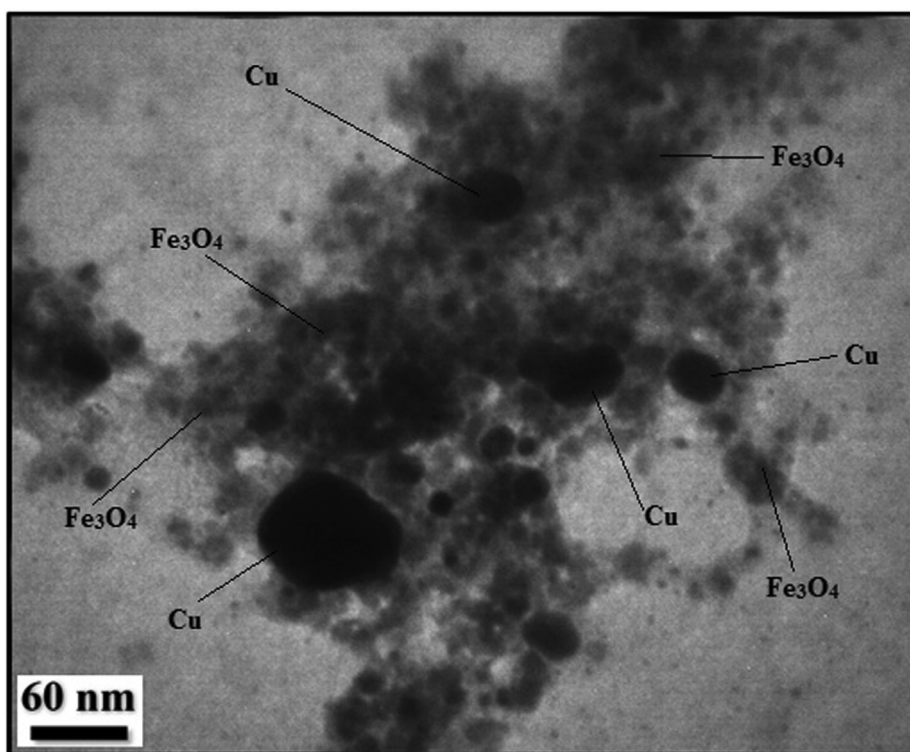
Fig. 2 TEM image of Cu-*Hibiscus*@Fe$_3$O$_4$ nanocomposite.
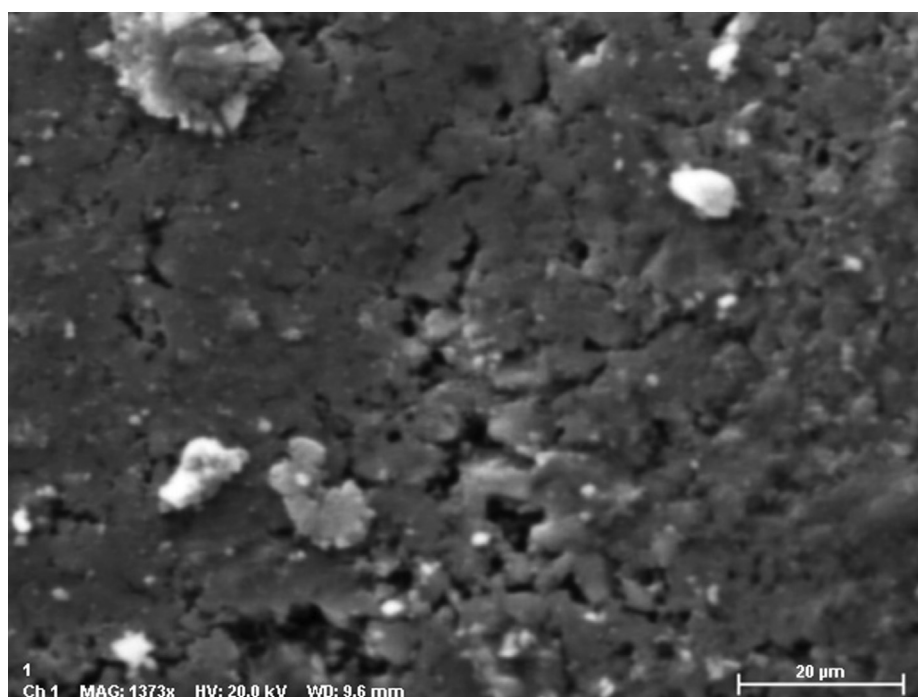
Fig. 3 SEM image of Cu-*Hibiscus*@Fe$_3$O$_4$nanocomposite.

external magnet and the solid compound obtained was filtered off. It was further purified by recrystallization from hot EtOH. All the products were reported previously and thus we determined their melting points and matched with authentic data.

2.5. Antioxidant analysis

An equal volume of DPPH free radical solution (0.04 mg/mL, 150 μL) was mixed to 5 different concentrations (31.25, 62.5,
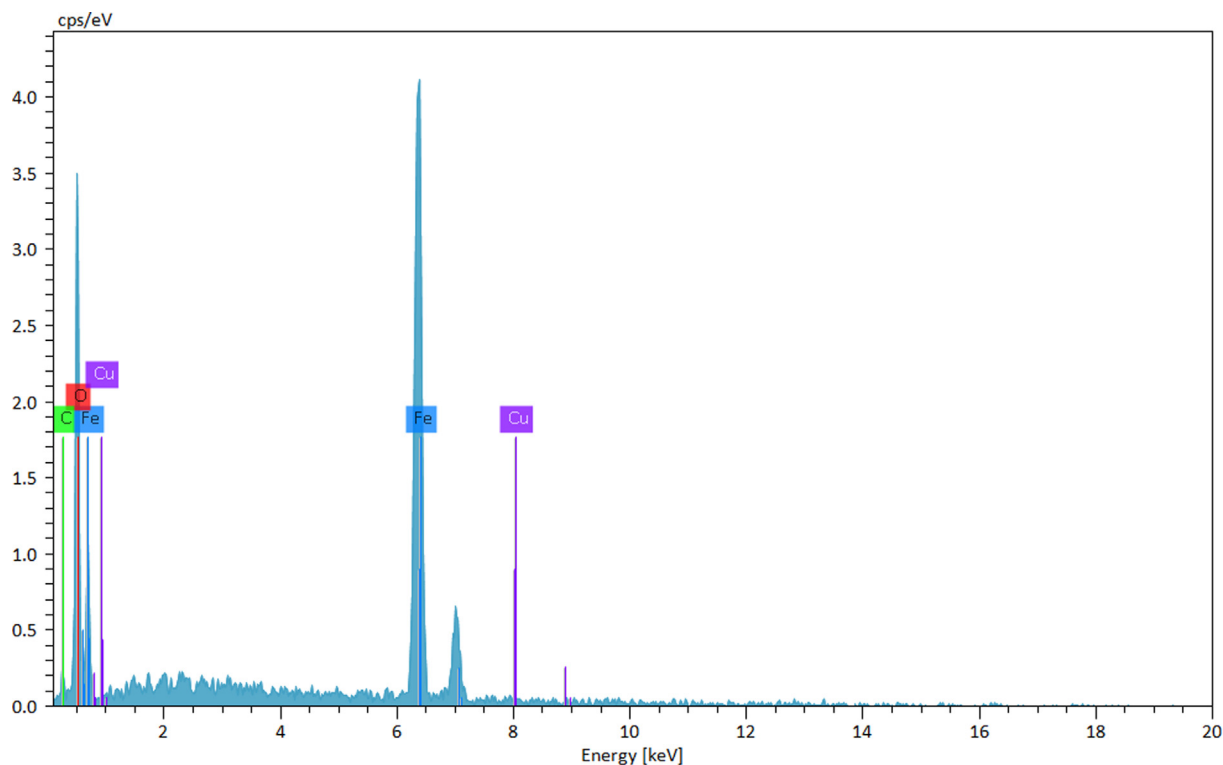
Fig. 4 EDX spectrum of Cu-*Hibiscus*@Fe$_3$O$_4$ nanocomposite.

125, 250, 500 and 1000 µg/mL) of the nanocomposite and subsequently incubated for 30 min. Absorbance of the corresponding mixtures were measured at 517 nm and the following equation was used to calculate the radical scavenging activity in terms of % inhibition.

$$Inhibition\ (\%) = \left(1 - \frac{Abs_{sample} - Abs_{blank}}{Abs_{control} - Abs_{blank}}\right) \times 100 \qquad (1)$$

Abs sample: absorbance of the reaction mixture, *Abs blank*: absorbance of the blank for each sample dilution in DPPH solvent, *Abs control*: absorbance of DPPH solution in sample solvent.

2.6. MTT assay

The cell lines were initially cultured in 96-well plates at 37 °C in 5% CO$_2$ atmosphere for 24 h. The growth media (10% FBS) was then decanted off from the plate and were washed twice with PBS. The compounds were then introduced in different concentrations (0.5, 5, 50, 500, and 1000 µg/mL) in RPMI medium and the system was incubated again for 3 days. The MTT dye in PBS solution (10 µL, 5 mg/mL) was next added to each well and incubated again for 4 h. In the same way media was removed and replaced with 100 µL DMSO in each well. In order to assist the formazan crystal solubilization all the plates were gently swirled. Finally, absorbance of the resulting mixture was measured at 545 nm and % cell toxicity alongwith IC 50 were determined as the following formula.

$$Toxicity\% = (1 - \frac{mean\ \text{OD of sample}}{mean\ \text{OD of control}}) \times 100$$

$$Viability\% = 100 - Toxicity\%$$

3. Results and discussion

3.1. Characterization of Cu-*Hibiscus*@/Fe$_3$O$_4$ nanocomposite

This study describes an eco-friendly method for supporting of Cu NPs on the surface of magnetic Fe$_3$O$_4$ NPs using *Hibiscus sabdariffa* extract as reducing and stabilizing agent without using of any toxic reagents. The Cu-*Hibiscus*@Fe$_3$O$_4$ nanocomposite were synthesized following two steps, the plant modified Fe$_3$O$_4$ MNPs adsorbs Cu^{2+} ions on its surface and then in *situ* reduction and stabilization of the adsorbed ions by the extract (Scheme 1). After synthesis, the nanocomposite particles were collected by an external magnet and dried under vacuum. Atomic absorption spectroscopy revealed that the material contains 0.12 mmol g^{-1} copper. The structural, morphological and physicochemical properties of the nanocatalyst were determined by various analytical techniques including FT-IR, SEM, EDX, TEM, ICP-OES, VSM and XRD study.

Fig. 1 displays the collective FT-IR spectra of pristine Fe$_3$O$_4$ NPs, *Hibiscus sabdariffa* extract and the Cu-*Hibiscus*@Fe$_3$O$_4$ nanocomposite. Fe$_3$O$_4$ NP is characterized by two broad bands at 1622 and 3420 cm^{-1}, being ascribed to the O-H bending vibrations from surface adsorbed water molecules and the O-H stretching vibrations of surface hydroxyl groups. Again, the peaks observed at 440 and 584 cm^{-1} are the characteristic of octahedral bending and tetrahedral stretching vibration of the Fe-O-Fe. The peak appeared at 633 cm^{-1} corresponds the cubic spinel ferrite structure. Conversely, in Fig. 1b, representing the FT-IR spectrum of the *Hibiscus* extract, several organic functional group bond vibrations are being observed, such as, O-H stretching (3400 cm^{-1}), C-H stretching (2929 cm^{-1}), C=C stretching (1622 cm^{-1}),
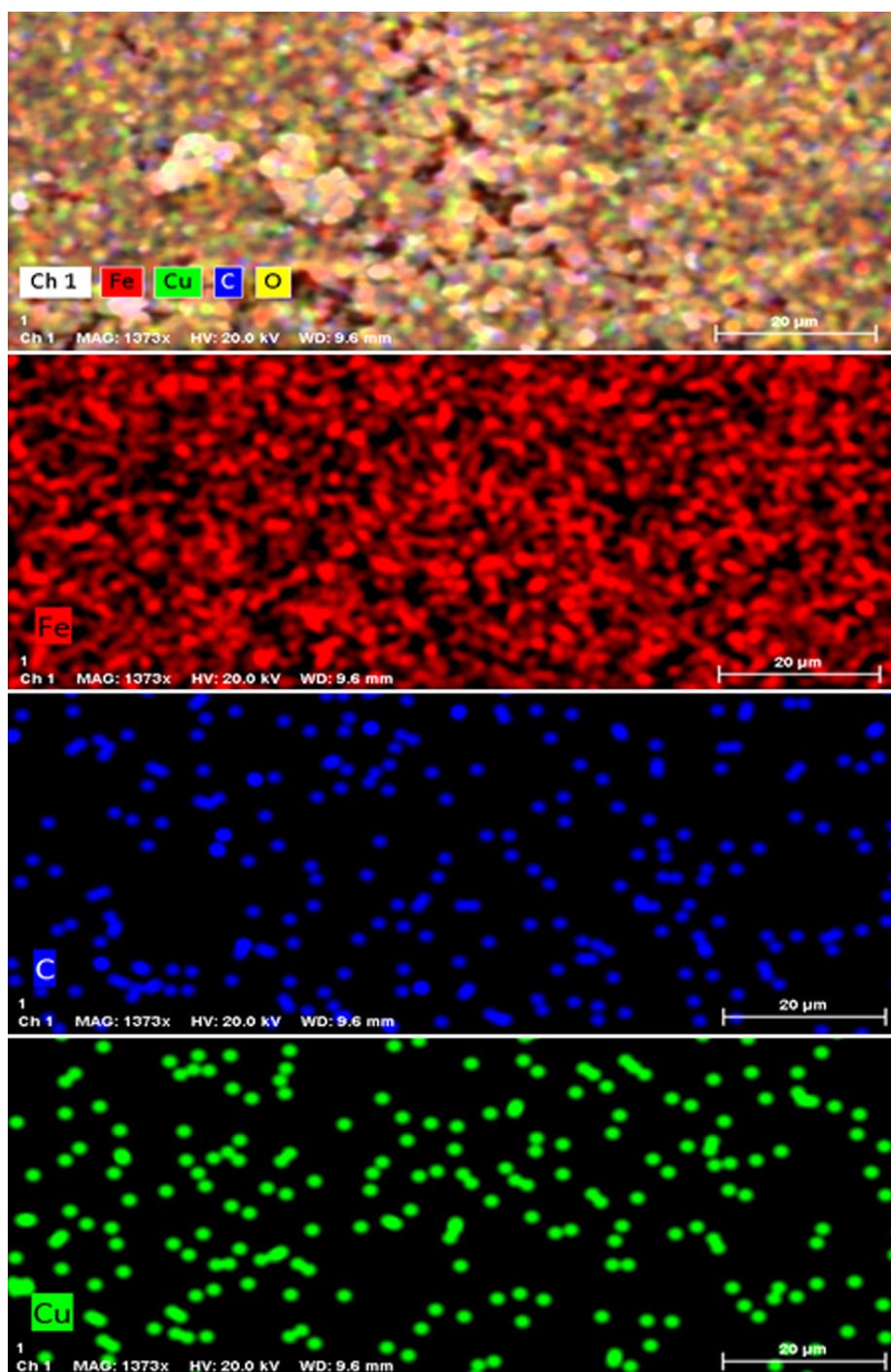
Fig. 5   SEM image of Cu/Fe_3O_4 nanocomposite with its elemental mapping.

C-O stretching (1259 cm^{-1}) and C-O-C stretching (1053 cm^{-1}). These peaks validate the presence of polyols, flavonoids, flavanols, tannins, terpenoids and organic acids in the flower extract. Finally, in the FT-IR spectrum Cu-*Hibiscus*@Fe_3O_4 nanocomposite (Fig. 1c), the overlapping of previous two spectra can be detected which is indicative of successful attachment of the two components. However, slight shift in the peaks can be detected in Fig. 1c as compared to the others, which can be anticipated due to the attachment of Cu NPs with the organofunctional moieties and ferrite hydroxyl groups.

In order to have an idea of structural morphology, shape and size of Cu-*Hibiscus*@Fe_3O_4 nanocomposite, the electronic microscopic analysis (TEM and SEM) were performed (Figs. 2 and 3). The particles are of globular shape. The grey and black particles represent the Fe_3O_4 and Cu NPs. Cu NPs are larger in size than the Fe_3O_4 NPs. Size of the particles of Fe_3O_4 and Cu NPs are 15–20 and 30–40 nm respectively. The surface modification by *Hibiscus sabdariffa* extract biomolecules over the core Fe_3O_4 NPs can be found from its shade like appearances. The homogeneous growth in the form of a thin layer of plant
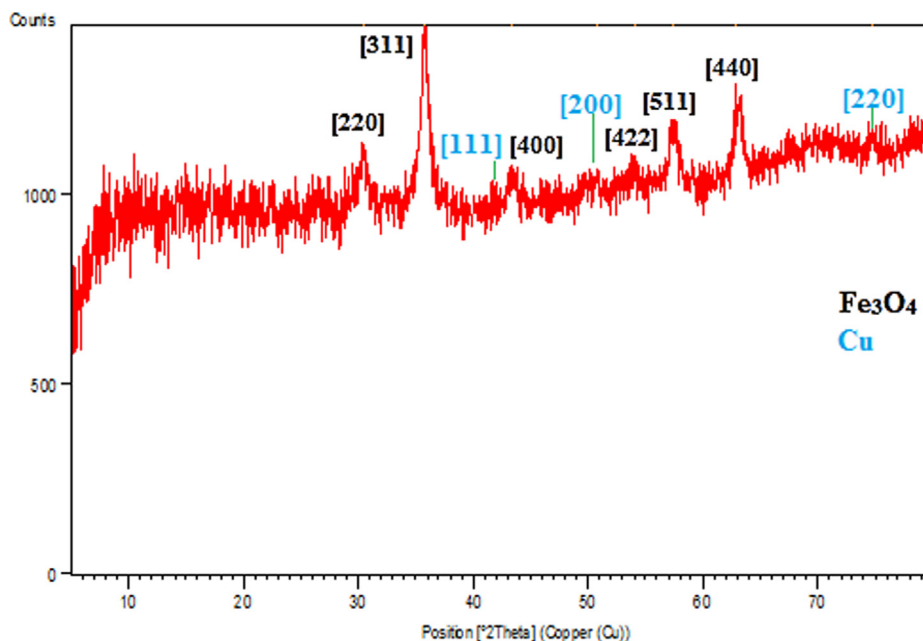
Fig. 6   XRD pattern of Cu-*Hibiscus*@Fe₃O₄ nanocomposite.

extract can be detected by close observation (Fig. 2). The nanometric and homomorphic size and uniform shapes of the primary (Fe₃O₄) and secondary (Cu) NPs definitely have synergistic effect on its catalytic activity. The high surface area of the material helps to bind the substrates and thereafter the active site serves the purpose by coupling the reactants together. The plant phytochemicals derived from *Hibiscus* extract also stabilizes the corresponding NPs not to agglomerate together, thus retaining their activity. However, from SEM image the phytochemical modification cannot be understood. The nanocomposite looks aggregated, possibly due to manual sample preparation (Fig. 3).

Chemical composition of the nanocomposite was assessed from EDX analysis and the profile is shown in Fig. 4. It represents Fe and Cu as metallic components. The occurrence of Cu confirmed the successful fabrication of Cu NP over the composite surface. Presence of C and O are the evidence of phyto-molecular attachments. The results were further justified by SEM elemental mapping analysis (Fig. 5). The compositional map reveals the Fe, C, and Cu species to exist with excellent dispersion throughout the matrix surface. Fine distribution of active species on the catalyst surface definitely has a significant effect on the catalytic activity. Architecture of the material can also be justified by the greater density of Fe species as compared to Cu, which indicates the denser core made of Fe.

Crystalline phases and the diffraction planes of the Cu-*Hibiscus*@Fe₃O₄ nanocomposite were ascertained by XRD study, that shown in Fig. 6. It represents a single phase profile indicating a united entity of the assembled counterparts. The typical diffraction peaks due to Fe₃O₄ are observed at 2θ = 30.2, 35.5, 43.4, 53.6, 57.2, 62.8° corresponding to (2 2 0), (3 1 1), (4 0 0), (4 2 2), (5 1 1) and (4 4 0) Bragg reflection planes respectively (JCPDS file, PDF No. 65-3107). Three

additional weak diffraction peaks observed at 2θ = 42.9, 49.8 and 75.3° are contributed from cubic crystalline Cu NPs being assigned to the (1 1 1), (2 0 0) and (2 2 0) planes, respectively. These peaks are evidently not from CuO phase, as evident from earlier reports (Joseph et al., 2016).

VSM study was carried out to determine the magnetic properties of the Cu-*Hibiscus*@Fe₃O₄ nanocomposite. On passing an external magnetic field of −20 kOe to + 20 kOe, a magnetic hysteresis curve is obtained and the corresponding saturation magnetization (*M*s) value of Cu-*Hibiscus*@Fe₃O₄ nanocomposite was 43.5 emu/g (Fig. 7). It clearly reveals the material to be superparamagnetic in nature. Even after the surface modification by non-magnetic plant extract and Cu NPs, the material was sufficiently magnetic to be attracted by an external magnet.
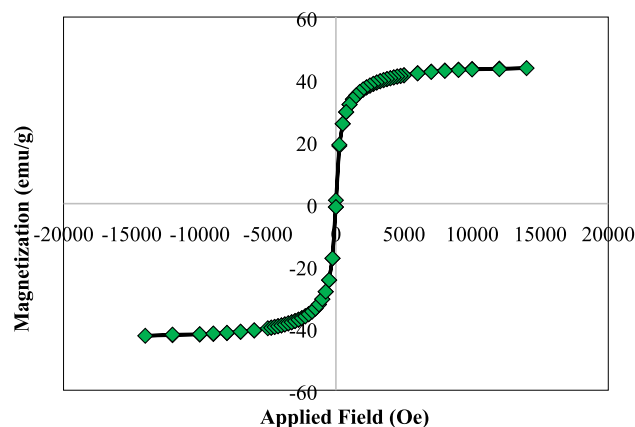
Fig. 7   VSM analysis of Cu-*Hibiscus*@Fe₃O₄ nanocomposite.

Table 1 Optimization of the reaction conditions for the synthesis of pyrano[3,2-*c*]chromene derivatives using the Cu-*Hibiscus*@Fe$_3$O$_4$ catalyst.[a]
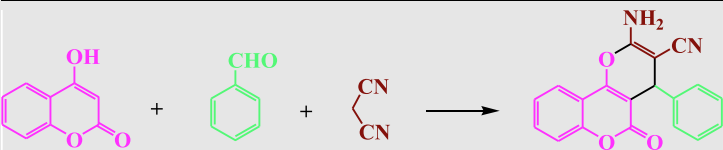
Entry	Solvent	Catalyst (mg)	Temp.	Time (h)	Yield (%)
1	EtOH	20	80 °C	3	70
2	hexane	20	70 °C	3	35
3	CH$_3$Cl	20	60 °C	4	45
4	CH$_2$Cl$_2$	20	40 °C	4	50
5	Toluene	20	110 °C	3	65
6	CH$_3$CN	20	82 °C	3	70
7	**H$_2$O**	**20**	**100 °C**	**3**	**90**
8	H$_2$O	30	100 °C	3	90
9	H$_2$O	10	100 °C	4	75
10	H$_2$O	20	25 °C	6	40
11	H$_2$O	0	100 °C	12	25

[a] Reaction conditions: 4-hydroxycoumarin (1 mmol), aldehydes (1 mmol), malononitrile(1 mmol), and solvent (5 mL) in the presence of Cu-*Hibiscus*@Fe$_3$O$_4$ catalyst.

3.2. The catalytic application of Cu-Hibiscus@Fe$_3$O$_4$ nanocomposite in the synthesis of pyrano[3,2-c]chromenes

When we had the all detailed characterizations of the Cu-*Hibiscus*@Fe$_3$O$_4$ nanocomposite,we explored the catalyst in the three component synthesis of pyrano[3,2-*c*]chromene derivatives (Scheme 1). In order to obtain the optimum reaction conditions, different parameters like the nature of solvent, amount of catalyst and temperature were applied on the one-pot condensation of 4-hydroxycoumarin, malononitrile and benzaldehyde in presence of Cu-*Hibiscus*@Fe$_3$O$_4$ nanocomposite towards the synthesis of 2-amino-4-phenyl-4,5-dihydro pyrano[3,2-c]chromene-3-carbonitrile, as a probe reaction. The outcomes are documented in Table 1. The screening was started with the variation of solvents. Initially, the three substrates taken in equimolar proportion (1 mmol each) were heated at reflex temperature in presence of 20 mg of catalyst. Among the different solvents used like EtOH, hexane, CH$_3$Cl, CH$_2$Cl$_2$, toluene, acetonitrile and water (entries 1–7), the best result was achieved in water affording 90% yields in just 3 h

reaction time (Entry 7). Noticeably, 20 mg of catalyst was decided as optimum catalyst load among the different catalyst amounts (entries 7–9). On applying a higher load (30 mg), the reaction yield did not improve further (entry 8). This is also to mention that the reaction did not proceed at all under catalyst free condition even after run for a prolonged time (entry 11). Again, aiming towards lower energy consumptions and achieving further sustainable condition, we continued the reaction at room temperature using best solvent and catalyst amount. However, only a moderate yield was obtained (entry 10).

After having the optimized results in hand, the next obvious endeavor was to explore the scope and generality of those reaction conditions over a variety of substrates. In order of that, a series of aromatic and heteroaromatic aldehydes were treated with 4-hydroxycoumarin and malononitrile at standard conditions and the results are shown in Table 2. Interestingly, all the aldehydes bearing various electron-donating (Me, OMe, NMe$_2$, OH) and electron-withdrawing groups (NO$_2$, Cl, Br) were equally compatible under the said conditions affording very good yields (entries 1–11). Even, there was no effect on

Table 2 Cu-*Hibiscus*@Fe$_3$O$_4$ catalyzed synthesis of pyrano[3,2-c]chromene derivatives.[a]

Entry	Aldehyde	Time (h)	Yield (%)[b]	TOF (h^{-1})[c]	TON (h^{-1})[d]	Mp (°C)	Mp (°C)[ref]
1	C$_6$H$_5$CHO	3	90	300	900	256–258	255–257 (Baziar and Ghashang, 2016)
2	4-Me-C$_6$H$_4$CHO	4	85	212.5	850	256–258	255–257 (Baziar and Ghashang, 2016)
3	4-MeO-C$_6$H$_4$CHO	5	90	180	900	249–251	248–250 (Baziar and Ghashang, 2016)
4	3-NO$_2$-C$_6$H$_4$CHO	2	90	450	900	263–265	262–264 (Baziar and Ghashang, 2016)
5	4-Cl-C$_6$H$_4$CHO	2	96	480	960	258–260	259–261 (Baziar and Ghashang, 2016)
6	2-Cl-C$_6$H$_4$CHO	2	90	450	900	274–276	274–276 (Baziar and Ghashang, 2016)
7	4-N(Me)$_2$-C$_6$H$_4$CHO	4	85	212.5	850	225–227	225–227 (Baziar and Ghashang, 2016)
8	2-Br-C$_6$H$_4$CHO	3	88	293.3	880	293–295	294–296 (Pradhan et al., 2014)
9	2,4-Cl$_2$-C$_6$H$_3$CHO	2	92	460	920	260–262	260–262 (Baziar and Ghashang, 2016)
10	4-OH-C$_6$H$_4$CHO	4	85	212.5	850	274–276	265–267 (Baziar and Ghashang, 2016)
11	3-OH-C$_6$H$_4$CHO	5	90	180	900	269–271	268–270 (Baziar and Ghashang, 2016)
12	2-furylaldehyde	3	80	266.7	800	251–253	251–253 (Baziar and Ghashang, 2016)

[a]General procedure: 4-hydroxycoumarin (1 mmol), aldehydes (1 mmol), malononitrile(1.0 mmol), Cu-*Hibiscus*@Fe$_3$O$_4$ (20 mg), H$_2$O (5 mL) at 100 °C; [b]Yield of isolated product; [c]TOF, turnover frequencies (TOF) = (Yield/Time)/Amount of catalyst (mol); [d]TON, turnover number (TON) = Yield/Amount of catalyst (mol).
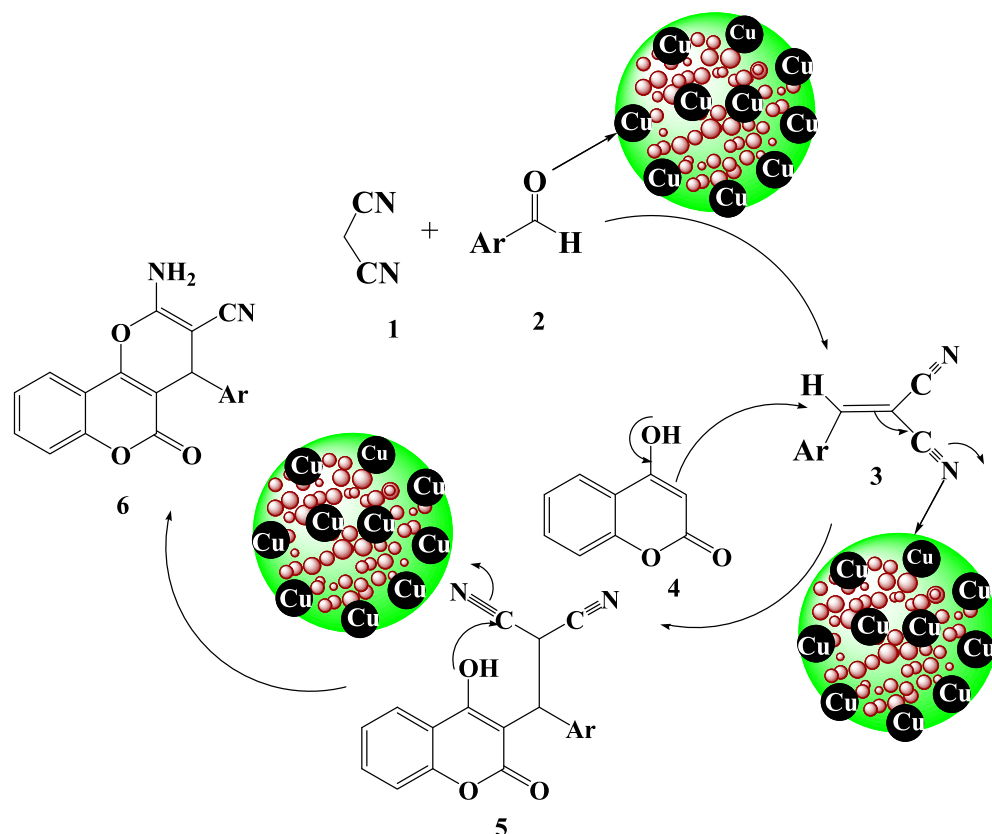
Scheme 2   Proposed mechanism for the synthesis of pyrano[3,2-c]chromene.

the geometric position of the substituent. In addition to aromatic aldehydes, heterocycle like 2-furfural was also stable under the reaction conditions and produced good yields (entry 12).

Regarding the mechanism, it is believed that malononitrile (1) and the aromatic aldehyde (2), being catalyzed over the material, undergoes Knoevenagel condensation initially to generate the intermediate 3. Another reactant, 4-hydroxy coumarin (4), subsequently adds up to activated 3, following Michael addition. The so generated Michael adduct (5), goes through internal cyclocondensation leading to the final product pyrano[3,2-c]chromene (6), leaving behind the catalyst for recycling (Scheme 2).

In heterogeneous green catalysis, the effortless isolation and reusability of catalyst is an elementary aspect. Accordingly, after completion of a fresh catalyzed probe reaction under optimized conditions, excess hot EtOH was added to dissolve the product and the catalyst was retrieved magnetically, washed well with EtOH (70%) and dried for reuse in further cycles. Interestingly, we could use the catalyst for 8 consecutive runs got with almost intact catalytic reactivity, as can be seen from Fig. 8. In order to validate the heterogeneity of the catalyst, hot filtration test was carried out with the probe reaction. When the reaction was on its half way time (90 min), it was stopped and the catalyst was isolated out of the reaction mixture. The conversion in this point of reaction was just 62% and the reaction filtrate was then allowed to run catalyst free for another 90 min. Noticeably, there was no additional or improved yield further. This also justified that no active Cu species had leached to the reaction mixture which could carry

the reaction forward, which in turn establishes the material as a true heterogeneous catalyst. Also, the FTIR spectra of the reused Cu-Hibiscus@Fe$_3$O$_4$ catalyst after 8 runs (Fig. 9) confirmed the stability of catalyst.

3.3. Study of antioxidant potential of Cu-Hibiscus@Fe$_3$O$_4$ nanocomposite

At the outset of our cancer studies over the Cu-Hibiscus@Fe$_3$-O$_4$ nanocomposite, we investigated the antioxidant efficiency of the material, as antioxidant potential is largely related to the cancer proliferation and apoptosis. The investigation was carried out through DPPH radical scavenging activity. The nanocomposite was introduced in six different concentrations, such as, 31.25, 62.5, 125, 250, 500 and 1000 µg/mL. Aqueous methanol (1 : 1) and BHT were considered as negative and positive controls respectively in the work. While scavenging
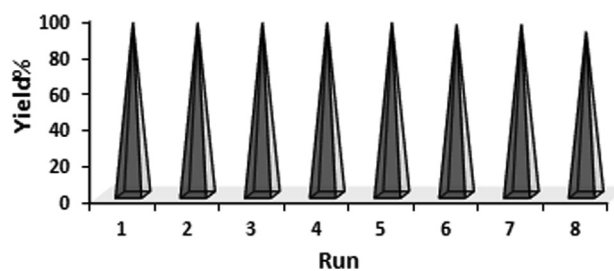
Fig. 8   The reusability of Cu-Hibiscus@Fe$_3$O$_4$ nanocatalyst.
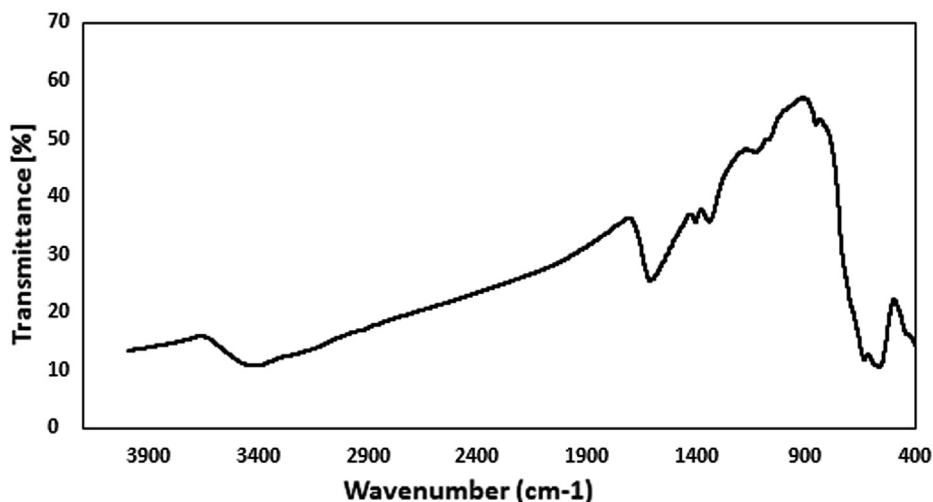
Fig. 9   The FT-IR spectra of reused Cu-*Hibiscus*@Fe_3O_4 nanocatalyst after 8 runs.

the DPPH free radical, the Cu-*Hibiscus*@Fe_3O_4 nanocomposite transfers an electron or hydrogen to it thus reducing the radical to a stable molecular species. This in turns results the fading out of initial deep purple color of DPPH to pale yellow. The scavenging capacity is thereafter measured thorough UV–Vis spectroscopy. UV absorbance (A) of the nanocomposite-DPPH complex at different concentrations were measured at 517 nm and antioxidant properties were calculated following equation (1). Evidently, the activity got enhanced with higher doses or concentrations and became highest at 1000 μg/mL (Fig. 10).

3.4. Cytotoxicity studies over Cu-Hibiscus@Fe₃O₄ nanocomposite

Standard MTT colorimetric assay was used in determining the cell viability and cytotoxicity of Cu-*Hibiscus*@Fe_3O_4 over the two colon cell lines HT-29 and Coca-2. The cells were treated with different concentrations of the material and observed for 48 h. Here also, the yellow MTT salt is reduced by the nanocomposite and the cell enzymes to form a purple for-

mazan crystal. This change in color is measured spectroscopically following absorbances of the dye treated cells at 545 nm. The Cu-*Hibiscus*@Fe_3O_4 nanocomposite showed very good cell viability on both the cell lines even up to 2000 μg/mL of its concentration (Figs. 11 and 12). As the cell toxicity is inversely related to % cell viability, the outcomes evidently displayed that the cell viability decreased dose-dependently over the catalyst. IC50 values of Cu-*Hibiscus*@Fe_3O_4 nanocomposite over the two cell lines were measured and found as 490.12 and 412.23 μg/mL, respectively (Table 3). The excellent colon resistance result of our developed material is believed to derive from their very good antioxidant potentials.

4. Conclusion

In summary, we demonstrate herein a unique biocompatible, plant phytochemical modified and magnetically isolable Cu nanocatalyst being successfully prepared by green method on the surface of Fe_3O_4 nanoparticles using *Hibiscus sabdariffa* flower extract. The *Hibiscus* extract had the function as a natural and green reducing agent of the immobilized Cu ions. The
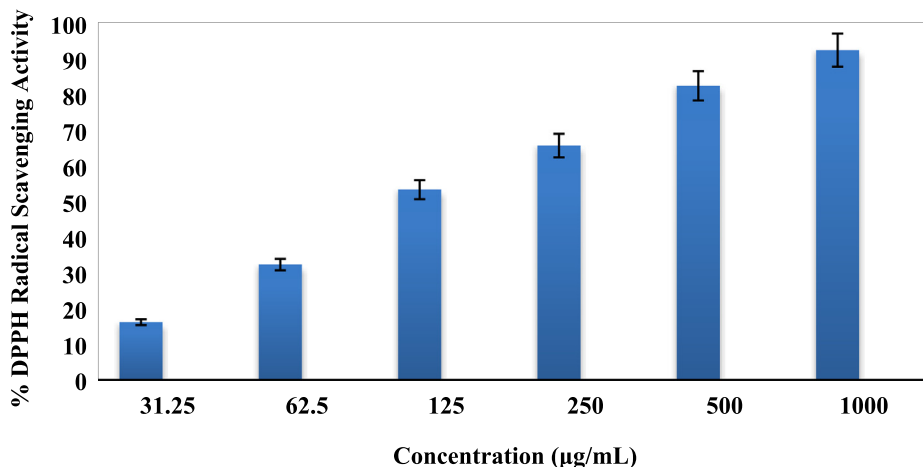
Fig. 10   Antioxidant activity of Cu-*Hibiscus*@Fe_3O_4 nanocomposite.
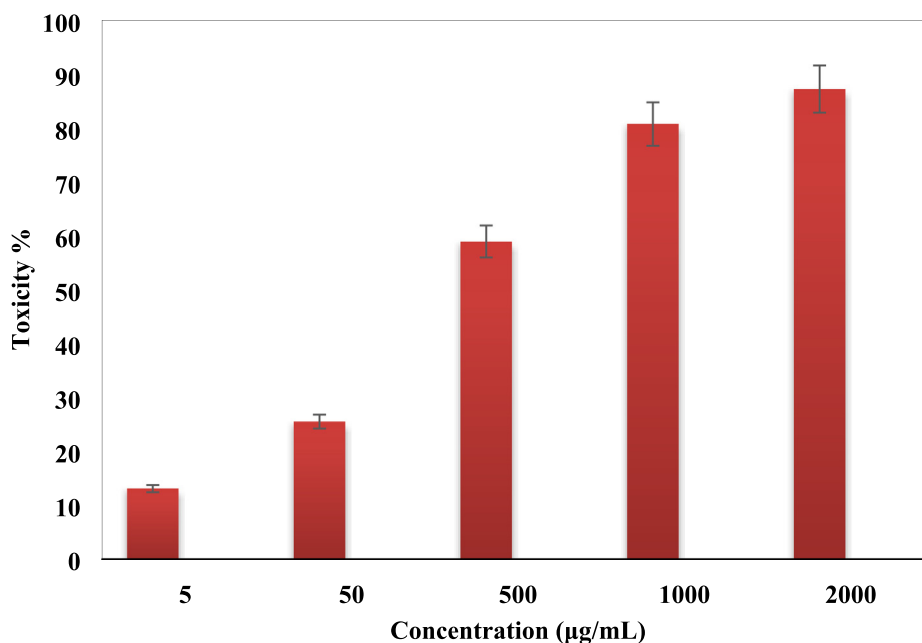
Fig. 11 *In vitro* toxicity analysis of Cu-*Hibiscus*@Fe$_3$O$_4$ nanocomposite on HT-29 cell.

synthesized Cu NPs at surface were found highly stable by the encapsulated plant phytochemicals. Such novel green nanocomposite was characterized by a wide range of analytical techniques. While exploring the catalytic applications, the Cu-*Hibiscus*@Fe$_3$O$_4$nanocatalystwas found highly effective in the multicomponent one-pot synthesis of diverse pyrano[3,2-c]chromenesby coupling 4-hydroxycoumarin, malononitrileand different aldehydesin refluxing aqueous media. It generated the products in high yields in short reaction time. The catalyst was subsequently isolated by simply using a magnet and the

products were collected by just filtration in pure form. The catalyst was regenerated by washing and drying and recycled eight successive times without considerable loss in its activity. Hot filtration test justified the true heteregeneity of the material as there was no considerable leaching of Cu in the solution. Additionally, the biological activities were measured by means of the inhibition activity of our material against the colon cancer cells. HT-29 and Coca-2 CRC cell lines were used to study the cytotoxicity, cell viability and antioxidant properties over our material and interestingly we achieved outstanding
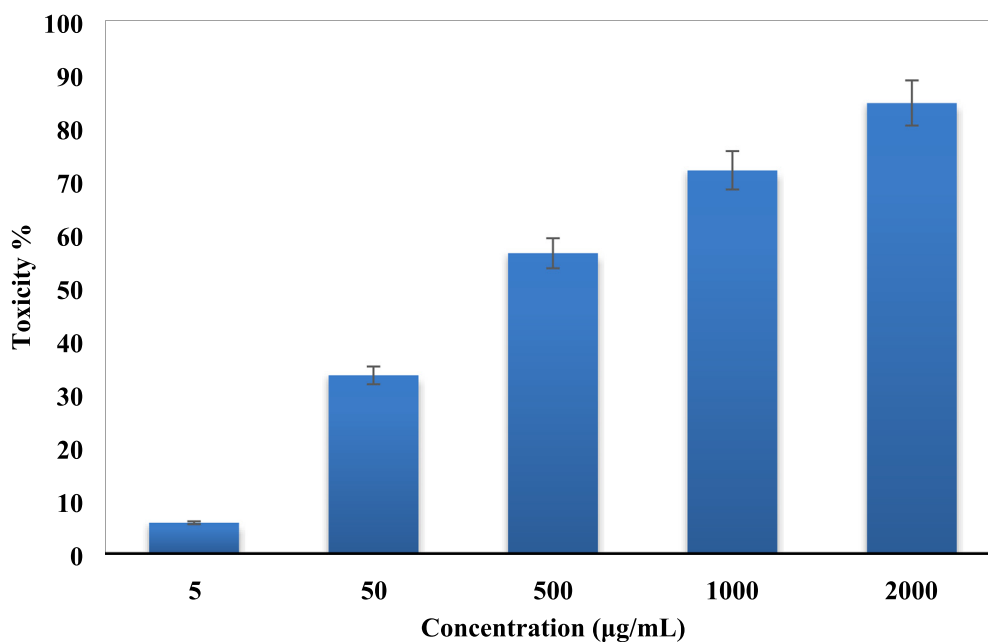
Fig. 12 *In vitro* toxicity analysis of Cu-*Hibiscus*@Fe$_3$O$_4$ nanocomposite on Coca-2 cell.

Table 3 The IC50 of Cu-*Hibiscus*@Fe$_3$O$_4$ nanocompositein the anti-human colon cancer test.

	Cu-Hibiscus@Fe$_3$O$_4$(μg/mL)
IC50 against HT-29	490.12 ± 0[a]
IC50 against Coca-2	412.23 ± 0[b]

decrease in cell viability dose dependently against the cell lines. The material also showed very good anti-oxidant properties as validated by the DPPH radical scavenging assay.

Contributions

All authors wrote, reviewed and edited the manuscript, analyzed the data, provided resources, were responsible for data curation, and reviewed drafts of the paper. All authors read and approved the final version of the manuscript.

Declaration of Competing Interest

The authors declare that they have no known competing financial interests or personal relationships that could have appeared to influence the work reported in this paper.

Acknowledgments

References

Abdel-Fattah, W.I., Ali, G.W., 2018. J. Appl. Biotechnol. Bioeng. 5 (2), 00116.

Adyani, S.H., Soleimani, E., 2019. Int. J. Hydrogen Energy 44, 2711–2730.

Aguilera, G., Berry, C.C., West, R.M., Gonzalez-Monterrubio, E., Angulo-molina, A., Arias-Carrión, Ó., et al, 2019. Nanoscale Adv. 1, 671–685.

Awual, M.R., Khraisheh, M., Alharthi, N.H., Luqman, M., Islam, A., Rezaul Karim, M., Rahman, M.M., Khaleque, M.A., 2018. Chem. Eng. J. 343, 118–127.

Baziar, A., Ghashang, M., 2016. React. Kinet. Mech. Catal. 118, 463–479.

Bisht, G., Rayamajhi, S., 2016. Nanobiomedicine 3, 1.

Bonsignore, L., Loy, G., Secci, D., Calignano, A., 1993. Eur. J. Med. Chem. 28, 517–520.

Brahmachari, G., Banerjee, B., 2014. ACS Sustainable Chem. Eng. 2, 411.

Burgard, A., Lang, H.J., Gerlach, U., 1999. Tetrahedron 55, 7555–7562.

Cao, X., Tan, C., Sindoro, M., Zhang, H., 2017. Chem. Soc. Rev. 46, 2660–2677.

Chetan, B.S., Nimesh, M.S., Manish, P.P., Ranjan, G.P., 2012. J. Serb. Chem. Soc. 77, 1–17.

Colombo, M., Carregal-Romero, S., Casula, M.F., Gutiérrez, L., Morales, M.P., Böhm, I.B., Parak, W.J., 2012. Chem. Soc. Rev. 41, 4306–4334.

Ding, Y., Shen, S.Z., Sun, H., Sun, K., Liu, F., Qi, Y., Yan, J., 2015. Mater. Sci. Eng. C 2015 (48), 487–498.

Dong, J., Li, J., Luo, J., Wu, W., 2019. Eur. J. Inflammation 17, 1.

Doustkhah, E., Rostamnia, S., Gholipour, B., Zeynizadeh, B., Baghban, A., Luque, R., 2017. Mol. Catal. 434, 7–15.

Esmaeilpour, M., Sardarian, A.R., Firouzabadi, H., 2018. J. Organometal. Chem. 873, 22–34.

Evans, J.M., Fake, C.S., Hamilton, T.C., Poyser, R.H., Showell, G.A., 1984. J. Med. Chem. 27, 1127–1131.

Gawande, M.B., Branco, P.S., Varma, R.S., 2013. Chem. Soc. Rev. 42, 3371–3393.

Ghashang, M., 2016. Res. Chem. Intermed. 42, 4191–4205.

Ghashang, M., 2016. Biointerface Res. Appl. Chem. 6, 1338–1344.

Ghashang, M., Mansoor, S.S., Aswin, K., 2014. Chin. J. Catal. 35, 127–133.

Ghashang, M., Kargar, M., Shafiee, M.R.M., Mansoor, S.S., Fazlinia, A., Esfandiari, H., 2015. Recent Pat. Nanotech. 9, 204–211.

Ghashang, M., Mansoor, S.S., Mohammad Shafiee, M.R., Kargar, M., NajafiBiregan, M., Azimi, F., Taghrir, H., 2016. J. Sulfur Chem. 37, 377–390.

Ghashang, M., Mansoor, S.S., Shams Solaree, L., Sharifian-Esfahani, A., 2016. Iran. J. Catal. 6, 237–243.

Gourdeau, H., Leblond, L., Hamelin, B., Desputeau, C., Dong, K., Kianicka, I., Custeau, D., Boudreau, C., Geerts, L., Cai, S.-X., et al, 2004. Mol. Cancer Ther. 3, 1375–1384.

Han, Y.D., Oh, T.J., Chung, T.H., 2019. Clinical Epigenetics 11, 51.

Hassanien, R., Husein, D.Z., Al-Hakkani, M.F., 2018. Heliyon 12, e01077.

Hemmati, S., Hekmati, M., Salamat, D., Yousefi, M., Karmakar, B., Veisi, H., 2020. Polyhedron 179, 114359–114364.

Hemmati, S., Heravi, M.M., Karmakar, B., Veisi, H., 2021. Sci. Rep. 11, 12362.

Heravi, M.M., AlimadadiJani, B., Derikvand, F., Bamoharram, F.F., Oskooie, H.A., 2008. Catal. Commun. 10, 272–275.

Heydari, R., Koudehi, M.F., Pourmortazavi, S.M., 2019. Chemistry Select 4, 531–535.

Jagadishbabu, N., Shivashankar, K., 2017. J. Heterocyclic Chem. 54, 1543–1549.

Joseph, A.T., Prakash, P., Narvi, S.S., 2016. Int. J. Sci. Eng. Technol. 4 (2), 463–472.

Khalilzadeh, M.M., Tajik, S., Beitollahi, H., Venditti, R.A., 2020. Ind. Eng. Chem. Res. 59, 4219–4228.

Khurana, J.M., Nand, B., Saluja, P., 2010. Tetrahedron 66, 5637–5641.

Lin, A., Zhang, J., Luo, P., 2020. Front. Immunol. 11, 2039.

Lotfi, S., Veisi, H., 2019. Mater. Sci. Eng. C 105, 110112–110122.

Makawana, J.A., Patel, M.P., Patel, R.G., 2012. Archiv Der Pharmazie 345, 314–322.

Maleki, A., Rabbani, M., Shahrokh, S., 2015. Appl. Organometal Chem. 29, 809–814.

Maleki, A., Akhlaghi, E., Paydar, R., 2016. Appl. Organometal Chem. 30, 382–386.

Maleki, A., Yeganeh, N.N., 2017. Appl. Organometal Chem. 31, e3814.

Maleki, A., Aghaei, M., Ghamari, N., 2016. Appl. Organometal Chem. 30, 939–942.

Maleki, A., Jafari, A.A., Yousefi, S., 2017. Carbohyd. Polym. 175, 409–416.

Maleki, A., Movahed, H., Ravaghi, P., 2017. Carbohyd. Polym. 156, 259–267.

Maleki, A., Hamidi, N., Maleki, S., Rahimi, J., 2018. Appl. Organometal Chem. 32, e4245.

Maleki, A., Hazizadeh, Z., Haji, R.-F., 2018. Micropor. Mesopor. Mater. 259, 46–53.

Maleki, A., Azadegan, S., Rahimi, J., 2019. Appl. Organometal Chem. 33, e4810.

Maleki, A., Varzi, Z., Afruzi, F.-H., 2019. Polyhedron 171, 193–202.

Maleki, A., Niksefat, M., Rahimi, J., Ledari, R.-T., 2019. Mater. Today Chem. 13, 110–120.

Maleki, A., Afruzi, F.-H., Varzi, Z., Esmaeili, M.S., 2020. Mater. Sci. Eng. C 109, 110502.

Mansoor, S.S., Logaiya, K., Aswin, K., Sudhan, P.N., 2015. J. Taibah Univ. Sci. 9, 213–226.

Mohammadi, P., Heravi, M.M., Sadjadi, S., 2020. Sci. Rep. 10, 6579–6588.

Mungra, D.C., Patel, M.P., Rajani, D.P., Patel, R.G., 2011. Eur. J. Med. Chem. 46, 4192–4200.

Olivera, S., Muralidhara, H.B., Venkatesh, K., Guna, V.K., Gopalakrishna, K., Kumar, Y., 2016. Carbohyd. Polym. 153, 600–618.

Patil, M.P., Kim, G.-D., 2017. Appl. Microbiol. Biotechnol. 101, 79.

Pradhan, K., Paul, S., Das, A.R., 2014. Catal. Sci. Technol. 4, 822–831.

Rahimi, J., Niksefat, M., Maleki, A., 2020. Front. Chem. 8, 615.

Rocha-Santos, T.A.P., 2014. Trends Anal. Chem. 62, 28–36.

Rostamnia, S., Doustkhah, E., 2015. J. Magn. Magn. Mater. 386, 111–116.

Rostamnia, S., Gholipour, B., Liu, X., Wang, Y., Arandiyan, H., 2018. J. Colloid Interface. Sci. 511, 447–455.

Rostamnia, S., Xin, H., 2014. Appl. Organometal. Chem. 28 (5), 359–363.

Rostamnia, S., Alamgholiloo, H., Jafari, M., 2018. Appl. Organometal. Chem. 32 (8), e4370.

Sadjadi, S., Mohammadi, P., Heravi, M.M., 2020. Sci. Rep. 10, 6535–6544.

Saundane, A.R., Vijaykumar, K., Vaijinath, A.V., 2013. Bioorg. Med. Chem. Lett. 23, 1978–1984.

K. Shivashankar, L.A. Shastri, M.V. Kulkarni, V.P. Rasal, S.V. Rajendra, Phosphorus, Sulfur Silicon and the Related Elements 183 (2007) 56–68.

Shivashankar, K., Kulkarni, M.V., Shastri, L.A., Rasal, V.P., Rajendra, S.V., 2006. Phosphorus Sulfur Silicon and the Related Elements 181, 2187–2200.

Singh, M.S., Nandi, G.C., Samai, S., 2012. Green Chem. 14, 447–455.

Tamoradi, T., Veisi, H., Karmakar, B., Gholami, J., 2020. Mater. Sci. Eng. C 107, 110260–110270.

Tamoradi, T., Daraie, M., Heravi, M.M., Karmakar, B., 2020. New J. Chem. 44, 11049–11055.

Tamoradi, T., Mousavi, S.M., Karmakar, B., 2021. J. Iran. Chem. Soc. https://doi.org/10.1007/s13738-021-02241-9.

Tamoradi, T., Kiasat, A.R., Veisi, H., Nobakht, V., Beshatai, Z., Karmakar, B., 2021. Chem. Eng. 9, 106009–106019.

Tamoradi, T., Veisi, H., Karmakar, B., 2021. Sci. Rep. 11, 2734.

Tamoradi, T., Kal-Koshvandi, A.T., Karmakar, B., Maleki, A., 2021. Mater. Res. Exp. 8, 056101.

Vala, N.D., Jardosh, H.H., Patel, M.P., 2016. Chin. Chem. Lett. 27, 168–172.

Valeri, N., 2019. Cancer Res. 79, 1041–1043.

Veisi, H., Karmakar, B., Tamoradi, T., Hemmati, S., Hekmati, H., Hamelian, M., 1983. Sci. Rep. 2021, 11.

Veisi, H., Hemmati, S., Safarimehr, P., 2018. J. Catal. 365, 204–212.

Veisi, H., Tamoradi, T., Karmakar, B., Mohammadi, P., Hemmati, S., 2019. Mater. Sci. Eng. C 104, 109919–109927.

Veisi, H., Tamoradi, T., Karmakar, B., Hemmati, S., 2020. J. Phys. Chem. Solids 138, 109256–109262.

Veisi, H., Karmakar, B., Tamoradi, T., Tayebee, R., Sajjadifar, S., Lotfi, S., Maleki, B., Hemmati, S., 2021. Sci. Rep. 11, 4515.

Venkatesham, A., Rao, R.S., Nagaiah, K., Yadav, J.S., Jones, G.R., Basha, S.J., Sridhar, B., Addlagatta, A., 2012. Med. Chem. Commun. 3, 652–658.

Wang, H.-J., Lu, J., Zhang, Z.-H., 2010. Monatsh. Chem. 141, 1107–1112.

Zhang, R.-R., Liu, J., Zhang, Y., Hou, M.-Q., Zhang, M.-Z., Zhou, F., Zhang, W.-H., 2016. Eur. J. Med. Chem. 116, 76–83.